Vehicular Communications 35 (2022) 100473

Contents lists available at ScienceDirect

Vehicular Communications

www.elsevier.com/locate/vehcom

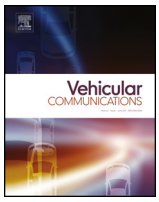

Multi-antenna 3D pattern design for millimeter-wave vehicular communications

Christian Ballesteros [a,*], Luca Montero [a], Germán A. Ramírez [a,b], Luis Jofre-Roca [a]

[a] Universitat Politècnica de Catalunya (UPC), Jordi Girona 31, Barcelona, 08034, Spain
[b] École Polytechnique Federale de Lausanne (EPFL), EPFL-STI-MAG, Bâtiment ELB, Station 11, Lausanne, CH-1015, Switzerland

ARTICLE INFO

Article history:
Received 7 September 2021
Received in revised form 27 March 2022
Accepted 18 April 2022
Available online 22 April 2022

Keywords:
V2X
Beamforming
Arrays

ABSTRACT

The transformation of the automotive industry towards ubiquitous connection of vehicles with all kind of external agents (V2X) motivates the use of a wide range of frequencies for several applications. Millimeter-wave (mmWave) connectivity represents a paramount research field in which adequate geometries of antenna arrays must be provided to be integrated in modern vehicles, so 5G-V2X can be fully exploited in the Frequency Range 2 (FR2) band. This paper presents an approach to design mmWave vehicular multi-antenna systems with beamforming capabilities considering the practical limitations of their usage in real vehicular environments. The study considers both the influence of the vehicle itself at radiation pattern level and the impact of the urban traffic on physical layer parameters. Connectivity parameters such as Signal-to-Interference-plus-Noise Ratio (SINR) and outage probability are optimized based on the array topology. A shaped beam in the vertical plane based on three preset radiating elements is proven to be robust enough against self-scattering effects on the vehicle body. Regarding the horizontal geometry, four panels on the roof's edges provide good coverage and link quality. The number of horizontal antennas per panel tightly depends on the required values of the link quality metrics, potentially leading to a non-uniform geometry between sides and front or back panels.

1. Introduction

The automotive industry is experiencing a transformation to shape the mobility of the future. Amid rising consciousness about its contribution to global pollution, and with a view to reduce the still large number of traffic accidents [1], connectivity and automation have emerged as key drivers of the industry's evolution towards greener, safer and more efficient transportation. This trend towards Connected and Automated Mobility (CAM) establishes new challenges to cope with connectivity-related issues such as assuring a certain Quality of Service (QoS) based on reliable and high-speed wireless links.

Although we are currently in an early stage of this evolution, vehicles are already equipped with a variety of sensors that assist the driver in taking decisions. Likewise, the so-called Advanced Driver-Assistance Systems (ADAS) often take control of some manoeuvres. However, safety-wise, vehicles just rely on ADAS as a mean to mitigate imminent road risks. In terms of connectivity, vehicles make use of back-end data to obtain useful information along the journey. New vehicles are also capable to connect to the Internet, but also connected road infrastructure is being deployed worldwide to help anticipating relevant information about unusual road conditions and potentially hazardous situations.

Intelligent Transportation Systems (ITS) make use of Vehicle to Everything (V2X) technologies, an umbrella term encompassing communications between the vehicle and the network, roadside infrastructure, pedestrians, and other vehicles. Early signs of successful V2X implementation have been experienced from 2019 onward [2], when the ITS ecosystem included support for a set of safety applications – namely, Day-1 use cases – in which nodes broadcast basic status messages to prevent road hazards. These V2X messages are to be transmitted with either IEEE 802.11p or Cellular V2X (C-V2X), technologies that coexist in the ITS Band (5.875 to 5.915 GHz) [3] harmonized for safety ITS.

The advent of advanced automotive use cases, with stringent requirements in terms of resource consumption [4,5], exemplify the need of enhanced features associated to New Radio (NR). Extended sensors or in-vehicle infotainment are expected to demand up to 1 GHz bandwidth with latency ranging between 3 and 50 ms and coverage up to hundreds of meters. In this context, although economically challenging for mass deployment, the use of the mmWave band (30-300 GHz), is essential to off-load the large volume of data required to realize the most demanding use cases.

* Corresponding author.
E-mail address: christian.ballesteros@upc.edu (C. Ballesteros).

https://doi.org/10.1016/j.vehcom.2022.100473

One of the mmWave well-established enablers is beamforming, consisting in feeding an array of antennas to obtain sharp beams of concentrated power towards the intended receiver/transmitter set. The high gain obtained helps overcoming the intrinsically large propagation losses of mmWave channels. In [6], the use of mmWave antenna arrays for V2X communications is addressed showing larger data capacity when the number of on-board antennas increases. However, even assuming seamless beam-alignment, beams should not be considered arbitrarily narrow just accounting for the potential gain and throughput, since antenna array behavior limits these possibilities.

Even though some studies apply appropriate beam distributions, like the pre-defined set of beams used in [7], most of the assumptions found in the literature use oversimplified antennas where beamwidth and beam-steering are indiscriminately flexible, which is not the case in the performance shown by customary User Equipment (UE). Similarly, antennas and radiation patterns used in most works are rarely altered by the vehicle or their mounting location. In [8], radiation patterns show asymmetries depending on their position. In [9], the location of V2X antennas at 5.9 GHz is optimized, pointing its importance on the performance of the communications, whereas the authors in [10] conclude that channel capacity depends on antenna height and location. More recently, the 5G Automotive Association (5GAA) published a study regarding the use of distributed antenna systems for Fifth Generation of Mobile Communications (5G) vehicular communications [11]. Co-located geometries are compared with distributed ones for both side and Uu links at 6 GHz. In case of sidelink, the performance of distributed geometries is demonstrated to outperform co-located antennas in terms of coverage – achievable SINR – and signal blockage reduction. In [12], a measurement-based study on the achievable diversity of distributed antennas is also presented, as well as the channel dispersion under different scenario conditions, also at sub-6 GHz. More simplistic studies strictly based on the impact of the vehicular platform on a single-antenna radiation can be found in [13,14]. Also, the authors in [15–18] antenna designs with some degree of reconfiguration (at pattern or frequency level), but all designs still target sub-6 GHz, low-gain radiation.

Notwithstanding these results at lower frequency bands, only few studies have been found tackling these effects at mmWave, although the Third Generation Partnership Project (3GPP) has emphasized the need for accurate radiation models at these bands [19]. In [20], the coverage of several antennas mounted on a vehicle is studied based on their perceived path loss when the transmitting antenna is moved around the vehicle. There, the use of a distributed system at high positions (i.e., the roof) is envisioned as a potential solution for such users to reduce blockage effects. The authors in [21] already propose a multi-band antenna design for V2X application supporting both sub-6 GHz MIMO and mmWave beamforming. However, the proposal is evaluated independently from the vehicle and the environment. Similarly, in [22], a dual-band V2X antenna is proposed, but a moderate-directivity beam without steering capabilities is obtained.

In this work, a vehicular antenna system is tailored to meet the common requirements of mmWave V2X with a design methodology formulated to account for the effects of the vehicle on the radiation pattern and the surrounding traffic to optimize communication towards other vehicles. The results aim to serve as a reference design for antenna-aware V2X evaluations at mmWave, giving importance to feasible implementations and the potential interactions with the car and the scenario. The most similar approach found in literature is in [23], where a reconfigurable mmWave multi-beam panel is proposed to be located at both front and rear windshields of the vehicle. However, that design targets solely to the elevation problem and the study does not consider azimuth coverage nor the scattering effect of the vehicle. In the present manuscript, the elevation problem is solved with a synthesized pattern, whereas a complete azimuth coverage is studied depending on the number of panels and radiators in the horizontal plane.

2. Considerations for the design of mmWave V2X antenna systems

The comparatively narrow spectrum portions available at frequency bands below 6 GHz (sub-6 GHz) fall short at fulfilling automotive-grade requirements like reliability, especially due to the expected large volumes of data to be exchanged. For instance, at 5.9 GHz, LTE-V2X delivers an average of 60% Packet Reception Rate at 60 km/h in urban scenarios [24]. 5G-V2X is expected to increase this metric [4], but the 99.99% reliability needed by highly-automated applications like platooning or sensor information sharing [25] cannot be met considering the high channel utilization rate expected at sub-6 GHz V2X bands. This motivates the use of larger bandwidths available at mmWave frequencies.

A common misconception related to the use of mobile mmWave is that propagation losses are prohibitive. However, as it is true that free-space path loss (FSPL) scales with the second power of frequency, it is also true that the effective antenna aperture does so. Therefore the feared FSPL can be compensated without increasing antenna space regardless of the operation frequency. On the other hand, when real-life propagation factors such as multipath fading, shading by obstacles, and atmospheric effects (i.e., water vapor and oxigen absorption, or rain) are included, path losses increase can be from mild to dramatic depending on the specific frequency band [26]. Fortunately, we can take advantage of the fact that the physical size of radiating elements becomes smaller as frequency grows. This fact allows packing more antennas without dramatically increasing the overall space. This, in combination with ingenious array design, allows to overcome most of the propagation-related losses.

The inherently directive nature of mmWave channels fosters the use of high gain antenna systems to exploit either direct Line-of-Sight (LOS) or indirect Non Line-of-Sight (NLOS) paths with narrow beams towards the dominant incoming or outgoing wave direction [27]. This comes with the additional challenge of beam alignment that may lead to unacceptable outage probabilities for arbitrarily narrow beams with low-accuracy, or low-rate beam updates [28]. Given this potential source of signal impairments, gain and beamwidth need to be carefully designed, as they are strictly related to the number of antenna elements in the array. Unless sophisticated methods are used, it is not feasible to assume low-cost and low-complexity vehicular arrays with focusing and defocusing capabilities to adapt their beam according to the channel state. Flexible arrays and fine phase resolution would lead to increased costs in the Radio Frequency (RF) processing, and robust phase shifters would be required [27]. It is also worth mentioning undesired effects such as sidelobes or scattering on the vehicle body when the beam is steered far from the broadside. All those considerations must be carefully depicted and addressed when designing an adequate geometry of the antenna array.

Conventional monopoles placed on the rooftop are widely used to obtain omnidirectional radiation patterns in vehicles at sub-6 GHz bands. However, the directional nature of the intended links at mmWave motivates a different antenna system topology, as in the absence of strong multi-paths, and given the channel losses, power radiated in unintended directions is practically lost. Therefore, vehicular beamforming antenna systems at mmWave must henceforth be arranged for sectorized coverage, each handled by a different array, to achieve an aggregated effective coverage similar to that of the monopole in the lower frequencies. Antenna arrays have a limited steering range with stable single-beam radi-

Table 1
Multi-panel antenna configurations supported by 3GPP Rel. 16.

Antenna ports	Panels	Antenna element distribution in array
8	2	
16	2	
	4	
	2	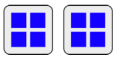
32	2	
	4	
	2	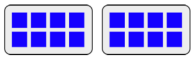
	4	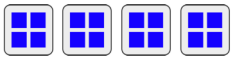

ation, outside of which increased sidelobes and potential grating lobes increase undesired radiation and reduce gain.

5G conceives these systems as multi-panel antennas, giving support to a set of virtual antenna configurations [29] shown in Table 1 [30] – notated here as N (columns, horizontally) $\times$ M (rows, vertically) antenna elements per panel. 5G support currently allows for a maximum of 32 controllable feeding weights to map on each antenna element, enabling up to 16 cross-polarized antenna elements. In the table, the configurations backed by the 3GPP are classified according to the number of panels (K) and antenna ports ($2 \times N \times M \times K$). For equal amount of ports, different geometries are allowed given the number of panels by arranging the antennas accordingly on each panel. The so-called codebooks establish the weights for each antenna port and therefore define a pre-configured set of beams steered to different angles.

Regarding coverage, it is reasonable to conceive the challenge of mmWave V2X antennas as separated in vertical and horizontal problems. On the vertical plane (i.e., in elevation, el), the goal is ensuring proper coverage of vehicles and infrastructure. It is safe to assume that vehicles will be in small elevation values ($el \simeq 0°$), whereas infrastructure will generally be around $0° < el < 30°$. Infrastructure appearing at higher el angles is assumed closer in distance and less radiated power can be assigned to those directions. On the horizontal plane (i.e., in azimuth, az), the required angles to reach the surrounding nodes will be relatively fast-changing, and no difference between azimuths can be easily set for coverage. Thus a vehicular beamforming antenna system can then be designed with steering capabilities to cover the entire horizontal plane, while having a suitable fixed configuration on the vertical plane. Arrays, thus, can be as simple as Uniform Linear Arrays (ULA).

3. Methodology

The use of mmWave for mobile communications poses several concerns on the allocation of antenna resources on the UE end of the link. The proposed methodology obeys both performance and cost-awareness criteria to evaluate different array designs. The parameters to analyze include the number of panels (arrays) on the car, the number of antenna elements per panel, and their most suitable location on the car.

Initially, an analytical study of the array geometry is performed based on the achievable array factor for both elevation and azimuth radiation. Then, the electromagnetic simulation of the array radiation is carried out with Altair FEKO's Multi-Level Fast Multipoles Method (MLFMM) solver. A basic rectangular patch is used as radiating element and a customizable number of elements is placed for each array geometry. In order to make the numerical simulations as time-efficient as possible, the isolated array is first simulated with this method. Then its near-field is combined with the geometry of the car using an equivalent source consisting of an aperture of 81×81 infinitesimal dipoles located at the antenna boundaries and placed on each position to be analyzed. The large electric size of the vehicle at mmWave frequencies entailed the use of Physical Optics (PO) to obtain the far-field radiation of the entire structure. To further improve calculation time, the entire bodywork, windows and windshields are considered as Perfect Electric Conductor (PEC), a model supported by reported measurements of the reflection coefficient of glass at mmWave [31].

Table 2
Configuration of urban vehicular traffic modeling for the case scenarios under evaluation.

Description	9 blocks of Manhattan Grid
Channel model	3GPP TR 37.885 Urban LOS/NLOSv [34]
Lanes	2 in each direction
Lane width	3.5 m
Grid size	433 x 250 m
Simulation area	1299 x 750 m
Vehicle velocity	60 km/h
Intersection turn probability	Going straight: 50% Turning left: 25% Turning right: 25%

Finally, the simulated patterns are tested in a typical Manhattan urban environment to assess their link-level performance in 5G-V2X-like communications. For that purpose, two more tools are used: one for the traffic simulation and another one to obtain the wireless channel behavior between communicating pairs. On the one hand, the realistic traffic of the urban grid is obtained with Simulation of Urban Mobility (SUMO) [32]. It allows to launch several simultaneous vehicle trajectories considering the distribution of the streets and the rest of the environment. In the simulation, vehicles are dropped in a way that the distance between the rear bumper of a vehicle and the front bumper of the following vehicle in the same lane follows an exponential probability distribution where the mean is 2 m at the velocity configured in each corresponding lane. The size is assumed $5 \times 2 \times 1.5$ m for all vehicles, which is later used to determine whether other nodes in the scenario block the direct path between two communicating ends. The vehicles drive at 60 km/h along random trajectories within a grid made by 9 buildings that create orthogonal streets of 4 lanes each (2 per direction). More details about the scenario can be found in Table 2. In this study, traffic density is kept constant since the estimation of the interference level is not using traffic information. The impact of that parameter is mainly expected to degrade the link SINR while increasing channel usage, but further investigation of that issue may be required.

On the other hand, once the trajectories are obtained, the previously calculated radiation pattern is applied to each vehicle position to calculate the wireless channel coefficients between random pairs of vehicles with the Quasi Deterministic Radio Channel Generator (QuaDRiGa) tool [33]. It makes use of Geometry Based Stochastic Channel Model (GBSCM) to estimate the behavior of a wireless channel, provided that there is a suitable trade-off between repeatability, generalization and accuracy compared to ray-tracing simulators or purely statistical models. The proposed simulation framework takes the urban channel models in [34] to estimate the distribution of the scatterers and their angular contribution is then weighted by the radiation to be tested in each case and coherently added at the receiver side.

All proposals are evaluated and designed at 28 GHz because evaluation procedures by the 3GPP already consider this band for

all V2X combinations [34], and it is the first 5G mmWave band being deployed in selected cities and implemented in smartphones.

4. Design of the multi-antenna beamset

The design of the antenna system is first studied in terms of the required coverage. To maximize the radiation to intended directions of individual array elements, the initial step to propose an adequate antenna system is to find the most suitable location on the vehicle. Then, the problem is divided in two dimensions: vertical and horizontal. Finally, the designed pattern is evaluated with a real planar array to be mounted as a vehicular UE panel.

4.1. On-vehicle placement

The optimum placement of the antenna arrays is the first issue to be addressed before proposing a particular geometry. Radiating elements surrounding the vehicle bodywork are strongly influenced by the latter, so an adequate positioning is paramount. Antenna radiation of sub-6 GHz vehicular antennas is a topic that has been extensively studied in the literature. Typical single-element omnidirectional can be achieved with shark-fin or monopole structures on top of the roof. Some available literature presents the radiation characteristic of such antennas [35,36]. Other manuscripts discuss alternative antenna locations, still at conventional frequency bands. In particular, the authors in [8,37] propose diversity-enabling positions on the sides and roof of different vehicles. In [38], the radiation and coupling of more directive elements is also considered. Bumper antennas achieve better isolation, as expected. But the use of highly directive antennas is able to compensate that issue even in the case of roof panels, achieving very low coupling factors.

In mmWave V2X, the use of multi-element beamformed patterns is implicit and they are particularly influenced by the environment in the proximity of the antenna. Additionally, full coverage is usually achieved with distributed geometries at different locations. As stated by the 5GAA in [11], typical implementations of Distributed Antenna Systems (DASs) consist of a central unit inside the vehicle and several antenna units around its bodywork. The latter can be implemented on the roof, with good azimuth coverage and clear view of high-elevation angles, or on the bumpers, glasses or mirrors, achieving more limited coverage. The sectorized disposition of such systems not only present aesthetic challenges but cable losses are also a concern for engineers. Antennas placed at the edges of the roof present a good balance of cable losses with regard to the other options and also can benefit from the curvature of these edges to promote an unnoticeable integration for any required antenna orientation. Antennas placed on the bumpers are limited to forward and backwards radiation, which is suitable for Cooperative Adaptive Cruise Control (CACC) [39]. Vehicle radars operating in the W band are commonly mounted on the front and rear bumpers for that reason, but alternative positions can be also a matter of study as in [40]. The surrounding bodywork poses additional issues in terms of signal blockage when the antennas are located there and this is partially studied in [20], where the path loss of a single radiating element on different positions along the vehicle is calculated. Then, placing antennas at the roof's edges can leverage some non-invasive parts for integration, such as the rear roof spoiler – where some vehicles already embed antennas – or the in-cabin rear-view mirror.

Fig. 1 illustrates a reference coordinate system originating in the roof's frontal edge position, where the orientation of the array is determined by the el_o angle that the normal of the array's surface points to. The orientation of the array has a strong influence on the achievable coverage, as later demonstrated in the following sections. In the case of a DAS, the same vertical orientation is kept for all available panels regardless of their position in the horizontal plane.

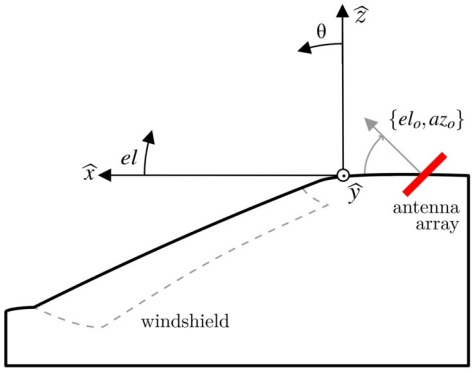

Fig. 1. Reference coordinate system.

4.2. Vertical plane coverage

As previously mentioned, a reasonable approach to solve the coverage challenges on the vertical plane is designing a suitable non-steerable beam that could give support for both Vehicle-to-Vehicle (V2V) and Vehicle-to-Infrastructure (V2I) links. For this purpose, Fourier synthesis is used for pattern design, being a widely acknowledged method that minimizes the Root-Mean-Square Error (RMSE) metric between the desired and synthesized beams [41]. In addition, the proposed arrays are to be located on the roof's edges following the criteria mentioned in the previous section.

The goal function to shape the desired vertical coverage is expressed in terms of the elevation Array Factor (AF), defined as a function of $\theta = 90° - el$, $-90° \leq el \leq 90°$. An optimized AF directly relates to the final beam radiation, following $\vec{E} = AF \cdot \vec{E_0}$, where $\vec{E}$ and $\vec{E_0}$ represent the electric field radiated by the array and the antenna element, respectively. Then, an appropriate beam for V2X applications can be pursued by designing an adequate goal AF. We define it as the following piece-wise function:

$$AF_{goal}(\theta) = \begin{cases} \cos(\theta_1)/\cos(\theta) & 0 \leq \theta < \theta_1 \\ 1 & \theta_1 \leq \theta \leq \theta_2 \\ 0 & otherwise \end{cases}, \quad (1)$$

where radiation is minimized for angles exceeding θ_2 to address the interfering reflections from the vehicle's body, while it is maximized for typical radiation directions, from θ_1 to θ_2. To avoid nulls when $\theta \to 0$, the AF is defined to be proportional to $\sec(\theta)$ in the range up to θ_1. Assuming a constant height for infrastructure nodes, this would compensate for the FSPL associated with distance.

To synthesize the goal function, the AF is described as a function of $\psi = kd\cos\theta + \alpha$ to capture the effects of inter-element spacing (d), frequency ($k = 2\pi f/c_0$), and progressive phase (α) [41]. For this method to work properly, $AF(\psi)$ must be specified over one entire period $|S_\psi| = 2\pi$, regardless of the size of the visible region. The followed procedure to obtain the weights to synthesize the goal function with is described by:

$$AF(\theta) \to AF(\psi_{\in(-\pi,\pi)}) \to AF(\psi_n) \to a_m \ , \quad (2)$$

where the a_M coefficients are a reduced set of the sampled array factor $AF(\psi_n)$ through an N_{pts} Inverse Discrete Fourier Transform (IDFT). The goal function can be fairly recreated by an odd number of antenna elements (M), arranged vertically and fed with a signal amplitude and phase dictated by the complex value of a_m. To

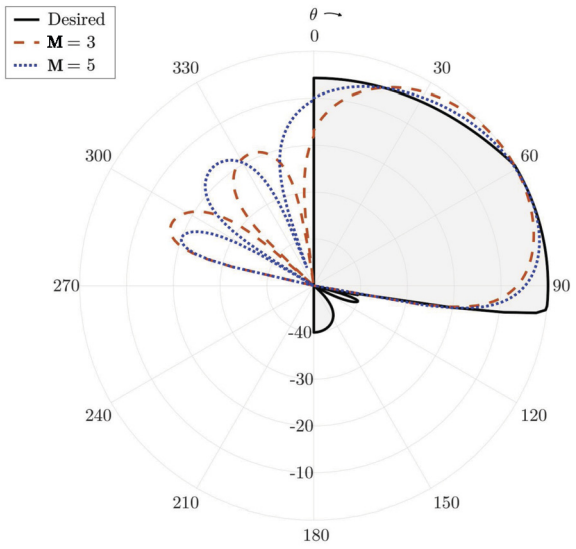

Fig. 2. Synthesized patterns with different number of array elements.

account for the possible antenna orientations, the synthesis is realized for different possible antenna pointing directions, aiming for the lowest RMSE, by rotating the goal AF according to the orientation being analyzed.

Then, a first analytical study is performed based on the achievable array factor with a variable number of antennas in elevation. This can be expressed with the following IDFT [41]:

$$AF(\psi) = \sum_{m=0}^{M-1} a_m e^{jm\psi} \tag{3}$$

The weights in (3) are those obtained from the Fourier synthesis of the piece-wise function described in (1).

$$a_n = \frac{1}{2\pi} \int_{-\pi}^{\pi} AF_{goal}(\psi) e^{-jn\psi} d\psi \tag{4}$$

The array synthesis on the vertical plane is set for the most restricting side of the car in terms of self-induced reflections: the front. In this case, the start of the established maximum for V2I is fixed as $\theta_1 = 60°$, according to typical V2I LOS angles. θ_2 is thoughtfully chosen depending on the angle at which reflections from the vehicle start being significant. This threshold is set as $\theta_2 = 105°$ for this vehicle model, giving a 5° margin to be generalized for other models.

The resulting goal AF can be reasonably synthesized with a small number of vertical elements. Fig. 2 represents the resulting theoretical pattern in elevation for 3 and 5 elements and the desired piece-wise function. In this case, the effect of the car is still not considered.

The RMSE of the synthesized solution compared to the goal AF is now calculated for $M = \{3, 5, 7, 9\}$ and for the whole range of $-90° \leq el_o \leq 90°$ with a 1° step. Those values for $el_0 < 0$ can be neglected, since the broadside direction of the array will be pointing directly towards the vehicle's bodywork, contrary to the design criteria to minimize its scattering. In this regard, the results in Fig. 3 point that increasing M shows little improvement on RMSE compared to the benefits of choosing the optimum el_o, especially considering the increased cost and complexity arising from a larger number of antenna elements. All the simulations find a local minimum for a certain el_{o_j}, which in all cases is very close to 80°, and suggest that the smallest number of antenna elements ($M = 3$) sufficiently fulfills the needs for cost-effective coverage.

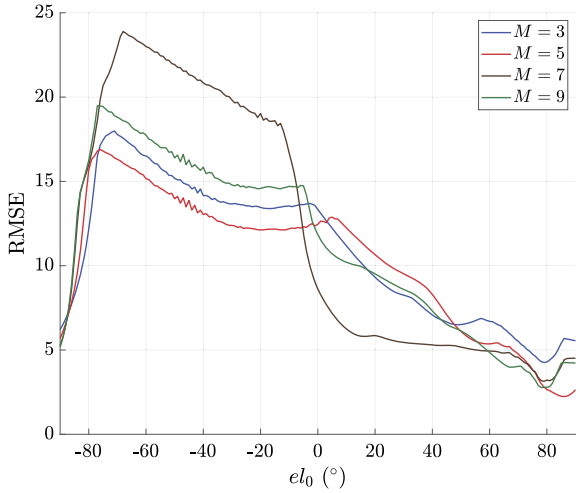

Fig. 3. RMSE in elevation varying array elements and tilt.

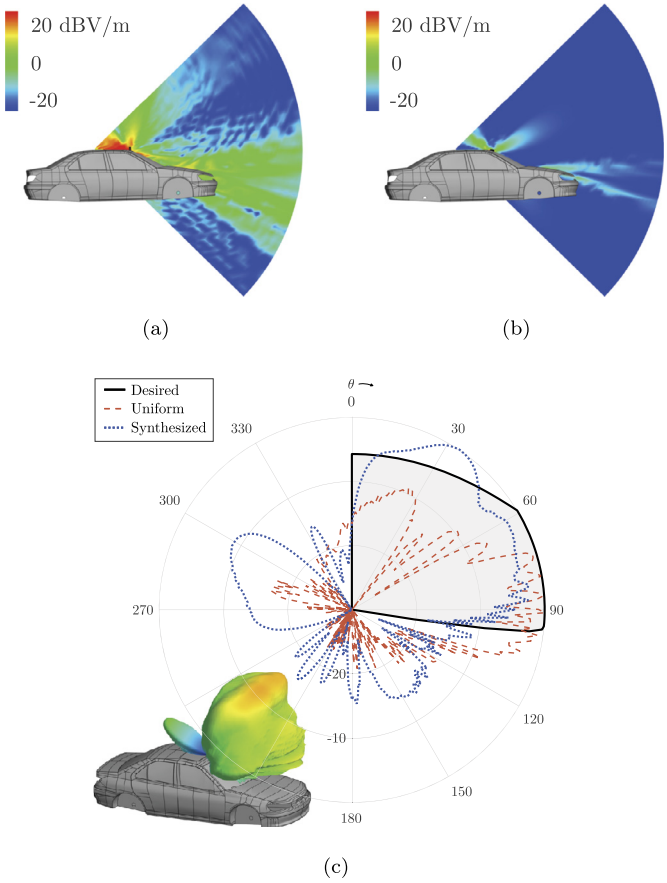

Fig. 4. Electric field scattered by the body of the vehicle when uniform feeding is applied in (a) and using the proposed 3-element synthesized pattern in (b). The overall front array radiation in presence of the vehicle is represented in (c).

To validate the suitability of the proposed solution, the scattered fields on the car of the proposed geometry with the optimized feeding and orientation are compared to those obtained with a uniformly fed array. Then, the radiation of the patch array mounted on the roof is numerically computed. As expected, the influence of the vehicle on the radiation pattern is substantially reduced as seen in Fig. 4. In Fig. 4a and Fig. 4b the distorting scattered fields due to the vehicle body are compared when uniform or the proposed synthesized feeding is used for 3 vertical antenna elements. The vertical radiation pattern accounting both for the

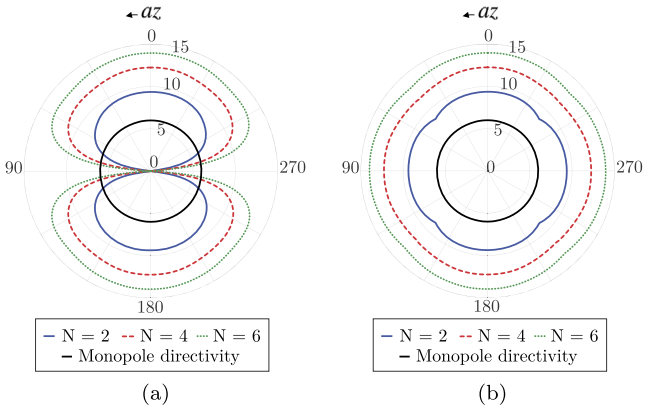

Fig. 5. Aggregated directivity for different N when (a) $K = 2$ and (b) $K = 4$ in the horizontal plane.

vehicle scattering and the array radiation is depicted in Fig. 4c. The desired AF is also shown as a reference. The main drawback of the synthesized pattern relates to the appearance of stronger back-radiation effect in the order of −9 dB compared to the maximum.

4.3. Horizontal plane coverage

Designing the optimum beam for the horizontal plane requires an additional knowledge on the propagation environment in which the vehicle is expected to communicate. As previously stated, sharp, high-gain beams will require complex, fast and accurate beam-alignment methods to prevent misalignments, but it could be a must to obtain large coverages for certain use cases.

As a first step, the horizontal coverage is studied in terms of the analytical aggregated radiation pattern in order to devise an adequate panel arrangement to use as baseline. To establish the configuration with lowest cost and complexity relying on the radiation pattern, a reasonable quality factor to validate can be based on obtaining monopole-like radiation, that is, being capable of an all-around coverage.

A convenient way to evaluate this monopole-like behavior is visualizing the aggregated radiation pattern, corresponding to the maximum envelope of the gains obtained for each steered beam enabled by the system. This is evaluated for the case of sectorized antenna systems with $K = \{2, 3, 4, 5, 6\}$ arrays (panels) with $N = \{2, 3, 4, 5, 6\}$ horizontal elements. For each K_i, the corresponding array is oriented towards $az_{o_{i,j}} = j \times 360°/K_i$, where $j = 0, 1, \ldots, K_i - 1$, to cover their corresponding sector with a required steering range of $360°/K_i$. Scenario evaluations suggest that $az \simeq \{0°, 90°\}$ are the most common Angle of Departure (AoD) or Angle of Arrival (AoA), so this formulation motivates that the frontal ($az_o = 0°$) and rear arrays ($az_o = 90°$) should be always present. The sectorized coverage of each panel is achieved with a predefined set of beams, i.e., a beamset, obtained with a Discrete Fourier Transform (DFT) codebook defined by the total number of horizontal elements [42,43]. For a phase-shifted DFT codebook with a center beam towards the broadside direction, the following expression is used:

$$a_n^l = \frac{1}{\sqrt{N_B}} \exp\left\{ -j \frac{2\pi n (l - \frac{N_B+1}{2})}{N} \right\} \tag{5}$$

where a_n^l denotes the weight of the n-th horizontal element when the l-th beam is to be created and N_B is an odd number of beams, so $l = 1, ..., N_B$. In this case, $N_B = N + 1$. For illustration, Fig. 5 presents the aggregated directivity for $K = \{2, 4\}$ and $N = \{2, 4, 6\}$

Table 3
Maximum scan loss (in dB) obtained with different array configurations.

N		2	3	4	5	6
K	3	1.9	1.5	1.0	0.9	0.8
	4	0.7	0.6	0.5	0.6	0.6
	5	0.3	0.4	0.4	0.5	0.4
	6	0.2	0.3	0.3	0.3	0.3

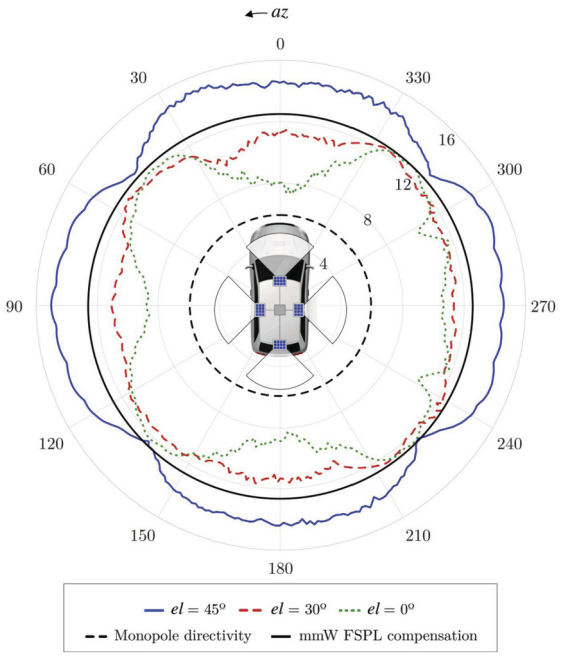

Fig. 6. Aggregated horizontal pattern for representative elevation cuts when the synthesized pattern is used together with a $K = N = 4$ and $M = 3$ configuration mounted on the vehicle.

when solely the array geometry without the influence of the vehicle is used. The simulated arrays are treated as horizontally-aligned ULAs, maintaining the independence between the horizontal and vertical problems. These plots showcase the broadening coverage as the number of arrays and antenna elements increase, using as a reference the maximum directivity of a conventional monopole, but also low directivity regions appear when the number of panels is small. The maximum scan loss perceived by the defined configurations within the steering range of each array is presented in Table 3. As seen in Fig. 5, the gain drops at the edge of the required steering range accentuates for smaller K, and improves for greater N, thus achieving smaller scan loss values. From $K \geq 4$, the scan loss does not substantially improve by increasing N, and even for $K = 4$ scan loss never exceeds 1 dB for any angle and N. This is directly reflected in the aggregated directivity variation, which presents a ripple smaller than 1 dB reflecting a monopole-like form factor.

Finally, the aggregated horizontal pattern for the case of $K = N = 4$ at different elevation angles when the array is placed on the vehicle roof's edges is presented in Fig. 6. The patterns are now calculated by means of numerical simulations with FEKO considering the antenna and the vehicle geometry. In the vertical plane, three elements are used to shape the beam proposed in Section 4.2 and the orientation of the arrays is $el_0 = 80°$. The maximum gain of the whole system is 14.6 dB, experienced in $(az, el) = (0°, 45°)$. This shows how the radiation pattern, despite the synthesis of the vertical coverage, presents the highest intensity at elevation values beyond the goal range. In any case, the gain in the $el = \{0°, 30°, 45°\}$ cuts always exceeds $\{12.4, 9.8, 7.4\}$ dB,

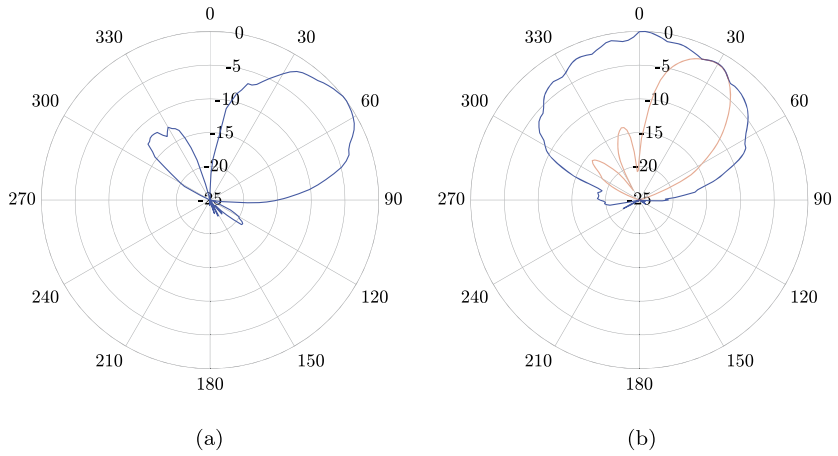

Fig. 7. Measured radiation of the antenna panel in (a) vertical and (b) horizontal planes.

respectively, thus achieving higher gains than a monopole (dashed circumference). The coverage also compensates the increased FSPL of mmWave compared to sub-6 GHz systems, as reflected in the reference circumference in Fig. 6. The solid black line indicates the gain increase needed to overcome the additional FSPL of moving from 5.9 to 28 GHz.

4.4. Experimental validation

The proposed antenna system is lastly validated by means of an experimental demonstration with an in-house manufactured antenna array. The module corresponds to one of the panels to be mounted on the roof of the vehicle. As stated below, the array must allow the user to horizontally steer the beam to achieve continuous scanning in the panel sector ($\pm$ 45°), while minimizing the scattering on the bodywork thanks to a shaped beam in the vertical dimension. In particular, $N = 4$ radiating patches are used in the horizontal plane, whereas $M = 3$ elements are vertically arranged to synthesize the desired pattern from Section 4.2.

The array radiation is measured in a controlled environment purposely built for the measurement of mmWave and THz antennas. The element weights are set thanks to a beamformer IC in the n257 5G band (the F5288 from Renesas Electronics). During the tests, the array acts as the receiving end and a reference horn is used as the transmitter at a distance of 900 mm to measure the far-field pattern.

Fig. 7 shows the measured normalized radiation in both vertical and horizontal planes of a single panel. The shape of the vertical beam approximates the theoretical pattern. However, the gain towards $\theta = 90°$ is degraded due to a narrower element radiation than expected (it must be reminded that the array is tilted 80°upwards in elevation). This issue must be addressed with a proper broadening of the beam for a successful coverage in V2V scenarios. Out-of-coverage radiation is limited below -12.2 dB to the maximum gain, corresponding to a backwards sidelobe. Regarding the horizontal pattern, a beamset composed of 9 beams covers 90°in azimuth with a maximum scan loss of 3.7 dB. Besides the aggregated pattern, one individual beam towards 30°is shown for instance. Sidelobes have a maximum normalized gain of -12.5 dB when the beamset is fixed at largest coverage angles.

5. Antenna system for mmWave V2V

From previous section, it is deduced that a 4-sector configuration with antennas on the roof's edges is an adequate trade-off between complexity and cost. In addition, the use of 3 antennas per RF chain with vertical beam shaping reduces the impact of scattered fields due to the vehicle body and induces better steering capabilities. However, the number of array elements in the horizontal plane is still open to discussion in light of the similar aggregated coverage regardless of N when $K = 4$. Then, different antenna solutions are provided and evaluated under realistic V2V channels to assess their suitability to maximize the quality of communications. V2V is chosen for this evaluation given its challenging quality assurance due to the fast varying channels. A similar approach could be carried out for V2I or Vehicle-to-Network (V2N), in which one of the communicating ends is static.

The support of 3GPP to manage this system is compatible with the vertical beam-shaping of the arrays, which is based on fixed feeding coefficients and can be set with pre-configured hardware and be transparent to the beamforming control. 5G codebooks for this multi-panel configuration constrain analog beamforming in the system to the horizontal plane, and define weights to obtain $O \times N \times M$ beams per panel – being O the DFT oversampling factor that defines the sweeping steps [44].

As stated in Section 3, each array configuration is tested in a realistic urban scenario where random vehicle pairs try to communicate using 5G-V2X-like links. Two visibility conditions are assumed: LOS and NLOS due to other vehicles (NLOSv) [34]. In total, up to $N_p = 1000$ vehicle pairs are simulated for TX-RX distances ranging from 20 to 250 m. For each pair, the best beam pair is determined with T_b periodicity by sweeping both beamsets and reporting the combination with maximum Reference Signal Received Power (RSRP). Given the large number of beams for high N values, an initial full-azimuth scan is performed when the link is established, but only a reduced set of $N_b = 5$ beams is used from that point forward. Along all trajectories, the perceived power by the receiving vehicle is calculated for the chosen beam pair. Then, assuming a certain 5G-V2X physical-layer configuration, it is possible to map those values to the SINR and, hence, an achievable throughput. No overhead is assumed in the calculation since it is not expected to differ between configurations when beam sweeping is performed for an equal N_b. All parameters concerning the simulations are depicted in Table 4.

For each link and time sample, the SINR is calculated assuming a noise power of $P_N = -174 + 10\log_{10} B + NF$ and a 2 dB margin accounting for additional interferences. This value is then translated to the maximum spectral efficiency supported by the current channel for a target Block Error Rate (BLER) with the following expression as in [45]:

$$\eta_{se} = \log_2\left(1 + \frac{1.5 \cdot \text{SINR}}{-\ln(5 \cdot \text{BLER})}\right) \tag{6}$$

Table 4
Configuration of the simulation environment.

Parameter	Symbol	Value
Simulation time		120 s
Sampling time	T_s	10 ms
Vehicle pairs	N_p	1000
Beam update period	T_b	{40, 80, 160} ms
Operating frequency	f_0	28 GHz
System bandwidth	B	50 MHz
MCS Table		Table 5.1.3.1-3 [30]
Target BLER		10^{-5}
Transmitted Power	P_T	20 dBm
Receiver Noise Factor	NF	13 dB
Array elements per panel	N	{2, 3, 4, 6, 8}
Beamset oversampling	O	2
Number of layers	l	1

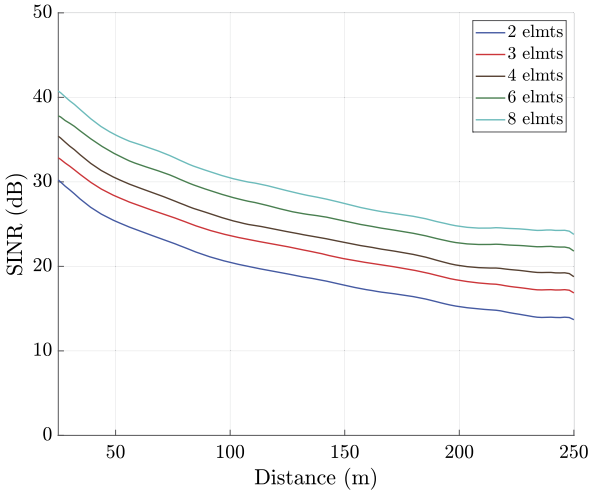

Fig. 8. Evolution of SINR as a function of distance for different number of array elements.

The experienced data rate is then adapted according to η_{se} so the link makes use of the maximum Modulation and Coding Scheme (MCS) level allowed by the channel. When no MCS is supported, the communication is interrupted and we call it as outage situation.

5.1. Average SINR

The first quality metric to validate is the SINR experienced by the receiver. For each V2V link and time sample, the received power and noise floor are calculated based on the values in Table 4. The beams are swept only with 40 ms period for now. The SINR calculated for all snapshots and trajectories is classified according to the distance between both vehicles and the mean value is calculated in for all samples within 2 m steps. The results are presented in Fig. 8 when 2 to 8 horizontal elements per panel are used. As expected, larger number of array elements imply an increased gain on both ends and hence more SINR in average. Doubling the number of elements provides up to 6 dB of improvement in total.

In the present work, the simultaneous use of equal or adjacent resources by several users in a crowded urban scenario is not considered. As previously stated, a 2 dB margin additional to the noise floor accounts for possible interference sources degrading the link quality at mmWaves. This might be particularly critical for distances below 100 m and small number of elements, for which the SINR at the receiver could be much lower than 20 dB and the performance of some advanced V2V use cases requiring large data rates (such as raw video and sensor data sharing or software updates [46]) could be compromised. It is worth mentioning that a 50 MHz channel bandwidth is used in the simulation. Increasing this value to 100 or even 200 MHz may help improving the achievable data rate at the expense of less available spectrum and higher noise power.

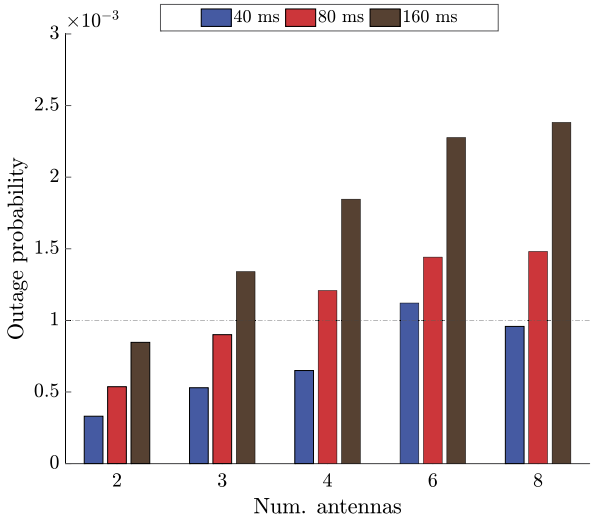

Fig. 9. Outage probability for different number of antennas per panel when the beam is updated every 40 (blue), 80 (red), and 160 ms (brown). The dashed line represents the 0.1% probability threshold.

5.2. Outage probability

The previous results regarding SINR could lead to the wrong impression that an arbitrarily large array is always beneficial to improve the quality of communications. However, a large amount of antennas is a challenge in terms of cost, complexity, and overhead efficiency. Thus manufacturers must guarantee the required performance with the minimum number of elements possible.

One key parameter to validate that is reliability. It is a broad term encompassing any behavior of the channel that degrades the signal quality. Despite Packet Reception Rate (PRR) is often used as the figure of merit, its usage implies higher-layer simulations under realistic network conditions. For the assessment of physical-layer parameters such as the number of antenna elements, it is deemed sufficient to estimate the outage probability. In the present work, it is defined as the probability of not supporting any available MCS of those defined by the 3GPP in Table 5.1.3.1-3 from [30], so no communication is possible. For a particular use case, this definition could be extended to the capability of supporting a certain MCS or data rate. An outage situation is given mainly for two reasons: either the peak gain of the array is not sufficient to overcome the channel losses or there is a beam misalignment due to slow beam update sweeping a large set of narrow beams. Fig. 9 shows the outage probability for a number of antennas per panel in the horizontal plane between 2 and 8 when the beam is updated every 40, 80, and 160 ms. As a reference, a black dashed line illustrates the 0.1% probability. It is clear from the results that large number of elements (e.g., 6 and 8) lead to sharper beams that can be easily misaligned, especially when beams are slowly updated. This is in accordance with the expected beam coherence time [6,47]. However, [47] defines statistical models to derive the temporal variation of a vehicular Rayleigh-faded channel when directional antennas are used. The channel is calculated for the 60 GHz band with a one-ring scatterer model for the NLOS component. This differs from the current work, where all results are based on numerical evaluations of a realistic urban scenario at 28 GHz.

Table 5
Mean time in outage for different number of antennas per panel and beam update period (units: ms).

N		2	3	4	6	8
Beam update	40 ms	49.4	51.1	26.5	38.7	29.7
	80 ms	52.5	34.3	38.7	41.7	39.8
	160 ms	57.0	47.4	58.5	59.9	58.4

Table 6
Mean beam duration on each panel (units: s).

N		2	3	4	6	8
Panel	Front	3.75	3.59	3.33	2.96	2.71
	Back	5.39	5.21	4.95	4.76	4.3
	Right	0.62	0.90	0.75	0.74	0.61
	Left	0.65	0.58	0.51	0.47	0.58

The effect of wider beams is not that evident. Very wide beams are expected to cover a very broad range of angles so large update periods could be sufficient. However, they suffer from low gain so large distances with high path loss at mmWave frequencies or any fading-related effect may cause large power drops impossible to overcome with such geometries. This issue is particularly evident in Table 5. There, the mean duration of an outage period for the same previous cases is depicted. When outage is produced due to low gain values (2 or 3 antennas per panel), it is not sufficient to increase the update rate and outage periods even larger than the update period are easily given. On the other hand, outage due to beam misalignments (sharp beams with high number of antennas, from 4 to 8) can be mitigated with faster updates.

5.3. Beam usage

The last parameter of interest is the mean duration of each beam, i.e., the time it takes in average for the car to switch to another beam, which can also be related to the beam coherence time. In this case, the values are classified by the panel being used. In this way, it is possible to discern which panels are prone to faster beam updates according to the traffic behavior in an urban scenario like the one under study. Table 6 shows the mean duration of a beam for panels ranging from 2 to 8 horizontal elements and the four panels on the roof's edges (front, back, right, and left, defined according to the driving direction). All values are calculated for a beam update period of 40 ms. As expected, the beams lasting longer time are those on the front and the back sides of the car. When two vehicles are driving on the same road, in the same or opposite direction, they tend to use similar beams until they reach each other. On the contrary, when a vehicle is overtaking or it crosses the other's path, lateral panels need to switch faster the beams. This is critical in situation of high-speed lanes like highways. In this case, all cars drive at an average speed of 60 km/h and even one order of magnitude difference is stated.

The results in Table 6 suggest that non-uniform panels or adaptive beams could provide better performance to prevent from outage when steering angles are close to the orthogonal of the driving direction. Focusing capabilities can be enhanced at front and rear angles with a large number of radiating elements, whereas wider beams made with less elements (and, hence, less costly solutions) are deemed to perform good enough sidewise. Then, up to 8 horizontal elements can be used in front and back panels given the large benefit in SINR, the low outage probability expected from front-to-back communications, and the similar performance in terms of outage when compared to 6 elements. For the side panels, vehicles communicating at those angles are usually closer as well, so there is no need of very high gain patterns and 3 elements should be sufficient as a trade-off between directivity and reliability.

6. Conclusions

In the present work, the benefits of appropriate choice of smart antenna arrays for Cooperative Connected and Automated Mobility (CCAM) is presented. Highly-reliable delivery of large data in a timely manner requires of large bandwidth channels available in mmWave frequencies and synchronization between vehicles. Beamforming capabilities are essential for that purpose but strong challenges appear such as beam alignment, strong shadowing effects, and scattering on vehicles that could degrade the intended beam performance. To help overcoming those issues, an adequate assessment of the antenna system mounted on the vehicles is required.

A cost-effective antenna system for mmWave vehicular communications is presented with beam steering capabilities in azimuth and a shaped constant beam in elevation to reduce scattering on the vehicle bodywork and to cover the necessary angles for V2X communications. The integration suitability on the vehicular platform is also studied. A 4-panel sectorized geometry with arrays mounted on the roof's edges is shown as an adequate trade-off between radiation properties, cost and integration. Regarding each array, only 3 vertical elements with fixed analog weights are able to provide fair enough radiation in elevation, which is maximum between $-15°$ and $30°$ and gain decreases in the $[30, 90]°$ range proportional to $\sec(90° - el)$.

On the horizontal plane, different solutions with a variable number of elements are studied. A predefined beamset covering all azimuth angles is used and its performance is validated through simulations on a realistic urban scenario where several V2V links are established. In light of the presented results, the proposed system obtains satisfactory all-around coverage to support a variety of connected vehicle applications foreseen in the autonomous landscape. The system aligns with 3GPP evaluation options for 5G-enabled vehicles, and the results show the possibilities of 5G codebooks applied to a mmWave antenna array operating in a V2V urban environment. The numerical simulation provides useful insights on the performance in terms of achievable SINR and outage probability for each case. A minimum number of 3 horizontal elements per panel properly satisfies both magnitudes. However, one could take advantage of the non-homogeneous distribution of traffic in azimuth to enhance the focusing capabilities to front and rear angles with an asymmetric geometry. There, up to 8 element could be mounted if the cost increase is still attainable.

Declaration of competing interest

The authors declare that they have no known competing financial interests or personal relationships that could have appeared to influence the work reported in this paper.

Acknowledgements

This work was partly funded by the Spanish Ministerio de Economía y Competitividad under the projects PID2019-107885GB-C31 and MDM2016-0600, the Catalan Research Group 2017 SGR 219, and "Industrial Doctorate" programme (2018-DI-084). The Spanish Ministry of Education contributes via a predoctoral grant to the first author (FPU17/05561).

References

[1] European Commission, Communication from the commission to the European Parliament, the council, the European economic and social committee, the committee of the regions - on the road to automated mobility: an EU strategy for mobility of the future (COM/2018/283 final), URL https://eur-lex.europa.eu/legal-content/EN/TXT/?uri=CELEX:52018DC0283, 2018.

[2] K. Sjoberg, P. Andres, T. Buburuzan, A. Brakemeier, Cooperative intelligent transport systems in Europe: current deployment status and outlook, IEEE Veh. Technol. Mag. 12 (2) (2017) 89–97.
[3] European Telecommunications Standards Institute (ETSI), ETSI TR 103 576-2. Pre-standardization study on ITS architecture; Part 2: Interoperability among heterogeneous ITS systems and backward compatibility, 2020.
[4] 5G Automotive Association (5GAA); Working Group Standards and Spectrum, Study of spectrum needs for safety related intelligent transportation systems - day 1 and advanced use cases, 2020.
[5] 3GPP, Technical Specification Group Services and System Aspects; Enhancement of 3GPP support for V2X scenarios; Stage 1 (Release 16), Technical Specification (TS) 22.186, 3rd Generation Partnership Project (3GPP), version 16.2.0, 06 2019..
[6] A. Pfadler, C. Ballesteros, J. Romeu, L. Jofre, Hybrid massive MIMO for Urban V2I: sub-6 GHz vs mmWave performance assessment, IEEE Trans. Veh. Technol. 69 (5) (2020) 4652–4662.
[7] F. Maschietti, D. Gesbert, P. de Kerret, H. Wymeersch, Robust location-aided beam alignment in millimeter wave massive MIMO, in: GLOBECOM 2017-2017 IEEE Global Communications Conference, IEEE, 2017, pp. 1–6.
[8] S. Kaul, K. Ramachandran, P. Shankar, S. Oh, M. Gruteser, I. Seskar, T. Nadeem, Effect of antenna placement and diversity on vehicular network communications, in: 2007 4th Annual IEEE Communications Society Conference on Sensor, Mesh and Ad Hoc Communications and Networks, IEEE, 2007, pp. 112–121.
[9] E. Whalen, A. Elfrgani, C. Reddy, R. Rajan, Antenna placement optimization for vehicle-to-vehicle communications, in: 2018 IEEE International Symposium on Antennas and Propagation & USNC/URSI National Radio Science Meeting, IEEE, 2018, pp. 1673–1674.
[10] N. Adhikari, S. Noghanian, Capacity measurement of multiple antenna systems for car to car communication, in: 2014 IEEE Antennas and Propagation Society International Symposium (APSURSI), IEEE, 2014, pp. 603–604.
[11] 5GAA, Distributed Vehicular Antenna Systems, Technical Report (TR), 5G Automotive Association, version 1.0, 01 2022.
[12] T. Abbas, J. Karedal, F. Tufvesson, Measurement-based analysis: the effect of complementary antennas and diversity on vehicle-to-vehicle communication, IEEE Antennas Wirel. Propag. Lett. 12 (2013) 309–312, https://doi.org/10.1109/LAWP.2013.2250243.
[13] A. Thiel, O. Klemp, A. Paiera, L. Bernadó, J. Karedal, A. Kwoczek, In-situ vehicular antenna integration and design aspects for vehicle-to-vehicle communications, in: Proceedings of the Fourth European Conference on Antennas and Propagation, 2010, pp. 1–5.
[14] J. Yang, J. Li, S. Zhou, Study of antenna position on vehicle by using a characteristic modes theory, IEEE Antennas Wirel. Propag. Lett. 17 (7) (2018) 1132–1135, https://doi.org/10.1109/LAWP.2018.2829718.
[15] L. Huang, Y. Lu, A switchable or MIMO antenna for V2X communication, in: 2019 IEEE International Conference on Computational Electromagnetics (ICCEM), 2019, pp. 1–2.
[16] K. Srivastava, A.K. Dwivedi, A. Sharma, Circularly polarized dielectric resonator-based multiple input multiple output antenna with pattern and polarization diversity for vehicular applications, Int. J. Circuit Theory Appl. 49 (10) (2021) 3421–3433.
[17] A. Zandamela, K. Schraml, S. Chalermwisutkul, D. Heberling, A. Narbudowicz, Digital pattern synthesis with a compact MIMO antenna of half-wavelength diameter, AEÜ, Int. J. Electron. Commun. 135 (2021) 153728.
[18] Z. Wang, S. Liu, Y. Dong, Compact wideband pattern reconfigurable antennas inspired by end-fire structure for 5G vehicular communication, IEEE Trans. Veh. Technol. (2022).
[19] Third Generation Partnership Project (3GPP), R1-1805259. V2X NR Evaluation Methodology - Suggestion for the incorporation of realistic vehicle antenna patterns, 2018.
[20] J.-J. Park, J. Lee, K.-W. Kim, K.-C. Lee, M.-D. Kim, Vehicle antenna position dependent path loss for millimeter-wave V2V communication, in: 2018 11th Global Symposium on Millimeter Waves (GSMM), IEEE, 2018, pp. 1–3.
[21] M. Ko, H. Lee, J. Choi, Planar LTE/sub-6 GHz 5G MIMO antenna integrated with mmWave 5G beamforming phased array antennas for V2X applications, IET Microw. Antennas Propag. 14 (11) (2020) 1283–1295.
[22] Y.-X. Sun, K.W. Leung, K. Lu, Compact dual microwave/millimeter-wave planar shared-aperture antenna for vehicle-to-vehicle/5G communications, IEEE Trans. Veh. Technol. 70 (5) (2021) 5071–5076.
[23] A. Nasr, K. Sarabandi, M. Takla, Multi-beam dual-polarized windshield antenna with wide elevation coverage for 5G V2X applications, in: 2020 IEEE International Symposium on Antennas and Propagation and North American Radio Science Meeting, 2020, pp. 1333–1334.
[24] Third Generation Partnership Project (3GPP), TR 36.885 V14.0.0. Study on LTE-based V2X Services, 2016, (Release 14).
[25] Third Generation, Partnership Project (3GPP), TR 22.886 V16.2.0. Study on enhancement of 3GPP Support, for 5G V2X Services, 2018, (Release 16).
[26] Y. Banday, G.M. Rather, G.R. Begh, Effect of atmospheric absorption on millimetre wave frequencies for 5G cellular networks, IET Commun. 13 (3) (2018) 265–270.
[27] S. Sun, T.S. Rappaport, R.W. Heath, A. Nix, S. Rangan, MIMO for millimeter-wave wireless communications: beamforming, spatial multiplexing, or both? IEEE Commun. Mag. 52 (12) (2014) 110–121.
[28] M. Giordani, A. Zanella, T. Higuchi, O. Altintas, M. Zorzi, On the feasibility of integrating mmWave and IEEE 802.11p for V2V communications, in: 2018 IEEE 88th Vehicular Technology Conference (VTC-Fall), IEEE, 2018, pp. 1–7.
[29] F. Henschke, Beamforming - how does it work, [Online]. Available: https://www.emf.ethz.ch/fileadmin/redaktion/public/downloads/3_angebot/veranstaltungen/AA_Henschke.pdf, Nov 2019. (Accessed 13 August 2021).
[30] 3GPP, Technical Specification Group Radio Access Network, NR, Physical Layer Procedures for Data, (Release 16), Technical Specification (TS) 38.214, 3rd Generation Partnership Project (3GPP), version 16.3.0 (09 2020).
[31] T.S. Rappaport, S. Sun, R. Mayzus, H. Zhao, Y. Azar, K. Wang, G.N. Wong, J.K. Schulz, M. Samimi, F. Gutierrez, Millimeter wave mobile communications for 5G cellular: it will work! IEEE Access 1 (2013) 335–349.
[32] P.A. Lopez, M. Behrisch, L. Bieker-Walz, J. Erdmann, Y.-P. Flötteröd, R. Hilbrich, L. Lücken, J. Rummel, P. Wagner, E. Wießner, Microscopic traffic simulation using SUMO, in: The 21st IEEE International Conference on Intelligent Transportation Systems, IEEE, 2018, pp. 2575–2582, https://elib.dlr.de/124092/.
[33] S. Jaeckel, L. Raschkowski, K. Börner, L. Thiele, QuaDRiGa: a 3-d multi-cell channel model with time evolution for enabling virtual field trials, IEEE Trans. Antennas Propag. 62 (6) (2014) 3242–3256.
[34] Third Generation Partnership Project (3GPP), TR 37.885 V15.3.0. Study on evaluation methodology of new Vehicle-to-Everything (V2X) use cases for LTE and NR, Release 15 (2019).
[35] P.W. Futter, L. Scialacqua, L.J. Foged, J. Soler, Combining measurement with simulation for automotive antenna placement and EMC analysis, in: 2018 IEEE 4th Global Electromagnetic Compatibility Conference (GEMCCON), 2018, pp. 1–4.
[36] M. Rütschlin, D. Tallini, Simulation for antenna design and placement in vehicles, in: Antennas, Propagation RF Technology for Transport and Autonomous Platforms 2017, 2017, pp. 1–5.
[37] D. Kornek, M. Schack, E. Slottke, O. Klemp, I. Rolfes, T. Kürner, Effects of antenna characteristics and placements on a vehicle-to-vehicle channel scenario, in: 2010 IEEE International Conference on Communications Workshops, 2010, pp. 1–5.
[38] K. Nono, M. Fujimoto, R. Yamaguchi, K. Tomimoto, A study on location of vehicle-mounted antennas for single-frequency full-duplex communication, in: 2021 International Symposium on Antennas and Propagation (ISAP), 2021, pp. 1–2.
[39] Z. Wang, G. Wu, M.J. Barth, A review on cooperative adaptive cruise control (CACC) systems: architectures, controls, and applications, in: 2018 21st international conference on intelligent transportation systems (ITSC), in: 2018 21st International Conference on Intelligent Transportation Systems (ITSC), 2018, pp. 2884–2891.
[40] A. Araghi, M. Khalily, P. Xiao, R. Tafazolli, Study on the location of mmWave antenna for the autonomous car's detection and ranging sensors, in: 2020 14th European Conference on Antennas and Propagation (EuCAP), 2020, pp. 1–4.
[41] Á. Cardama, J. Romeu, J.M. Rius, L. Jofre, S. Blanch, M. Ferrando, Antenas, Univ. Politèc. de Catalunya, 2004.
[42] L. Zhou, Y. Ohashi, Efficient codebook-based MIMO beamforming for millimeter-wave WLANs, in: 2012 IEEE 23rd International Symposium on Personal, Indoor and Mobile Radio Communications-(PIMRC), IEEE, 2012, pp. 1885–1889.
[43] Y. Huang, C. Liu, Y. Song, X. Yu, DFT codebook-based hybrid precoding for multiuser mmWave massive MIMO systems, EURASIP J. Adv. Signal Process. 2020 (1) (2020) 1–13.
[44] Third Generation Partnership Project (3GPP), R1-1612661, Advanced CSI Codebook Structure, 2018.
[45] H. Seo, B.G. Lee, A proportional-fair power allocation scheme for fair and efficient multiuser OFDM systems, in: IEEE Global Telecommunications Conference, GLOBECOM'04., Vol. 6, 2004, IEEE, 2004, pp. 3737–3741.
[46] 5GAA, Working Group Standards and Spectrum, Study of Spectrum Needs for Safety Related Intelligent Transportation Systems - Day 1 and Advanced Use Cases, version 1.0, Technical Report (TR) TR S 200137 5G Automotive Association, 06 2020.
[47] V. Va, J. Choi, R.W. Heath, The impact of beamwidth on temporal channel variation in vehicular channels and its implications, IEEE Trans. Veh. Technol. 66 (6) (2017) 5014–5029.